






# Metrics for Optimizing Searches for Tidally Decaying Exoplanets

Brian Jackson<sup>1</sup> , Elisabeth R. Adams<sup>2</sup> , and Jeffrey P. Morgenthaler<sup>2</sup> <sup>1</sup> Department of Physics, Boise State University, 1910 University Drive, Boise, ID 83725-1570 USA<sup>2</sup> Planetary Science Institute, 1700 East Fort Lowell, Suite 106, Tucson, AZ 85719, USA

Received 2023 May 24; revised 2023 August 7; accepted 2023 August 7; published 2023 September 5

## Abstract

Tidal interactions between short-period exoplanets and their host stars drive orbital decay and have likely led to engulfment of planets by their stars. Precise transit timing surveys, with baselines now spanning decades for some planets, are directly detecting orbital decay for a handful of planets, with corroboration for planetary engulfment coming from independent lines of evidence. More than that, recent observations have perhaps even caught the moment of engulfment for one unfortunate planet. These portentous signs bolster prospects for ongoing surveys, but optimizing such a survey requires considering the astrophysical parameters that give rise to robust timing constraints and large tidal decay rates, as well as how best to schedule observations conducted over many years. The large number of possible targets means it is not feasible to continually observe all planets that might exhibit detectable tidal decay. In this study, we explore astrophysical and observational properties for a short-period exoplanet system that can maximize the likelihood for observing tidally driven transit timing variations. We consider several fiducial observational strategies and real exoplanet systems reported to exhibit decay. We show that moderately frequent (a few transits per year) observations may suffice to detect tidal decay within just a few years. Tidally driven timing variations take time to grow to detectable levels, so we estimate how long that growth takes as a function of timing uncertainties and tidal decay rate and provide thresholds for deciding that tidal decay has been detected.

*Unified Astronomy Thesaurus concepts:* [Exoplanet dynamics \(490\)](#); [Star-planet interactions \(2177\)](#); [Transit timing variation method \(1710\)](#)

## 1. Introduction

From the discovery of the first exoplanet orbiting a Sun-like star (Mayor & Queloz 1995), orbital decay powered by tidal interactions has been a point of concern (Rasio et al. 1996). So close to their host stars, short-period gas giants raise substantial tidal bulges on their host stars, large enough that in some cases, the bulge has been detected (Barros et al. 2022). For host stars rotating more slowly than their short-period planetary companions revolve, the interaction between this tidal bulge and the planet transfers angular momentum from the orbit to the star, reducing the orbital distance and period (Jackson et al. 2008). The rate at which tidal energy is dissipated within the host star determines the orbital decay rate but, for stars on the giant branch, may be comparable to the stellar luminosity (MacLeod et al. 2018). The stellar dissipation processes, usually quantified via the tidal dissipation parameter  $Q_*$ , are likely complex and remain poorly understood (Ogilvie 2014), translating into orders of magnitude of uncertainty in  $Q_*$ .

Once a gas giant spirals into its Roche limit, a distance determined in part by the stellar and planetary densities (Rappaport et al. 2013), tidal disruption can occur. This disruption may proceed on a timescale set by the tidal decay rate (Valsecchi et al. 2015; Jackson et al. 2016), or the disruption may become unstable and proceed rapidly (Gu et al. 2003; Jia & Spruit 2017). Or, in a more dramatic case, the planet's Roche limit may lie within the star, and the tidally decaying planet can be directly accreted by the star (Metzger et al. 2012).

A variety of indirect observational evidence supports these theoretical expectations that short-period planets are disrupted and/or accreted by their host stars. Some stars show signs of tidal- or accretion-induced spin-up (Qureshi et al. 2018); main-sequence stars that currently host hot Jupiters tend to be younger, on average, than main-sequence stars that host planets less susceptible to tidal decay (Hamer & Schlaufman 2019); and some red giant stars exhibit anomalous chemical signatures that may be caused by planetary engulfment (Aguilera-Gómez et al. 2016), and such signatures may also be present but short-lived for main-sequence stars (Behrard et al. 2023). De et al. (2023) provided the first direct detection of ongoing planetary engulfment. Based on a large-scale survey, that study reported the detection of a low-luminosity optical transient lasting several days, accompanied by a months-long infrared brightening. These signatures are consistent with engulfment of a planet between 0.1 and 10  $M_{\text{Jup}}$  by a Sun-like star about 4 kpc from Earth.

Based on their survey detection statistics and other considerations, De et al. (2023) estimated that such events occur at a rate of between 0.1 and 1  $\text{yr}^{-1}$  within the Milky Way. As discussed in Metzger et al. (2012), the engulfment rate scales with  $Q_*$ ; a value of  $Q_* \sim 10^6$  translates into about one tidally driven planetary accretion event per year within the Milky Way. However, the large uncertainties on  $Q_*$  mean the actual event rate is likewise highly uncertain. Moreover,  $Q_*$  likely depends on stellar structure, with later-type stars exhibiting more efficient dissipation (smaller  $Q_*$ ), and probably also on tidal driving frequency.

One way to constrain  $Q_*$  and the galactic engulfment rate for exoplanet systems would be to observe tidally driven orbital decay, which would manifest as variations in transit timing. Unfortunately, tidal decay has only been definitively detected



Original content from this work may be used under the terms of the [Creative Commons Attribution 4.0 licence](#). Any further distribution of this work must maintain attribution to the author(s) and the title of the work, journal citation and DOI.

this way for one hot Jupiter, WASP-12 b (Patra et al. 2017; Yee et al. 2020). The period decay rate reported in Yee et al. (2020),  $dP/dt = -29 \pm 2 \text{ ms yr}^{-1}$ , translates to  $Q_* \approx 2 \times 10^5$  and amounts to a change in the period of just under half a second since the planet was discovered in 2008. A recent analysis of TESS data confirmed this decay rate, reducing the error bars below  $1 \text{ ms yr}^{-1}$  (Wong et al. 2022). Possible tidal decay has also been reported for several other systems, including XO-3 b (Ivshina & Winn 2022; Yang & Wei 2022), WASP-19 b (Patra et al. 2020; Ivshina & Winn 2022), TrES-1 b, TrES-2 b, HAT-P-19 b (Hagey et al. 2022), Kepler-1658 b (Vissapragada et al. 2022), and KELT-9 b (Harre et al. 2023). However, definitive confirmation will likely require additional years of observations, and knowing which planets to prioritize requires understanding how decay is detected and what parameters best suit a system to exhibit detectable decay.

Detecting tidal decay requires fitting an ephemeris to observed transit times. In the absence of tidal decay, the transit times are regularly spaced (by orbital period  $P$ ) and increase linearly with observational epoch  $E$ . When there is tidal decay, transits come faster and faster over time as the orbital period declines, and an additional quadratic term proportional to  $E^2$  and involving the period change  $dP/dE$  appears in the ephemeris. Deciding whether a series of transit times is better modeled with a linear ephemeris with no decay or a quadratic ephemeris with decay requires considering more than the standard reduced  $\chi^2$  (Press et al. 2002); the quadratic ephemeris can always, in principle, result in a smaller reduced  $\chi^2$  because it involves one more model parameter than the linear ephemeris.

In recent years, astronomers have invoked the Bayesian information criterion (BIC; Schwarz 1978) to judge whether a data set supports tidal decay. This simple expression incorporates both  $\chi^2$ , thereby favoring models that minimize residuals, and a term that penalizes introducing additional model parameters, thereby favoring lower-dimensional models. In this context, the BIC can be written as

$$\text{BIC} = \chi^2 + k \ln N, \quad (1)$$

where  $N$  is the total number of data points, and  $k$  is the number of fit parameters, 2 for a linear fit and 3 for a quadratic fit. Generally, when comparing two models, the one with the smaller BIC is favored. For a difference in BIC between two models,  $\Delta\text{BIC}$ , Yee et al. (2020) pointed out that the Bayes factor,  $B$ , i.e., the ratio of posterior probabilities favoring the linear (no tidal decay) to the quadratic (tidal decay) model, is given by

$$B = \exp(-\Delta\text{BIC}/2). \quad (2)$$

As an example, the collection of transit timing observations for WASP-12 b considered here give  $\Delta\text{BIC} \approx 200$ , favoring a model with tidal decay by a probability  $\sim 10^{43}$  times larger than a model without tidal decay. Given its utility, in this study, we explore the various system parameters and observational strategies that can promote detection of tidal decay, framing our analysis around the BIC.

We focus on the effects of tidal decay on a transiting planet’s ephemeris. However, other astrophysical processes can impact it as well. Orbital precession, for example, can accelerate the transit times, thereby mimicking the effects of tidal decay, at least as far as the transit is concerned (Patra et al. 2020). Observing a planet’s eclipse times can distinguish between

decay and precession, since the former will accelerate both transit and eclipse times, but the latter will accelerate one and decelerate the other. Both mechanisms, though, introduce curvature into the ephemeris (whether the transit or eclipse ephemeris), and the analysis presented here can be used to explore the detection of ephemeris curvature, whatever the cause (or sign). Future studies may better tailor this approach to searches for precession, line-of-sight acceleration (e.g., Deeg et al. 2008), or other ephemeris perturbations.

In what follows, we first explore what astrophysical properties for a planetary system best lend themselves to precise transit times (Section 2.1). Then, we consider the details of fitting both linear and quadratic curves in the cases of tidal decay and no tidal decay (Sections 2.2–2.4). Finally, we apply our formulation to several hypothetical observing programs and then to real observational data for a few systems with possible tidal decay (Section 3). Throughout the analysis, we invoke the WASP-12 system as a point of comparison. Since WASP-12 is the only system with definitively detected tidal decay, the evolution over time of the various detection statistics we explore here for this system serves as a template for detecting tidal decay in other systems.

## 2. Analysis

For our analysis, we considered data for hot Jupiter and short-period brown dwarf systems from the NASA Exoplanet Archive downloaded on 2023 April 5 and subject to the following requirements.

1. The planet must have “Published Confirmed” listed in the “Solution Type” column.
2. The planetary system must have listed the ratios of both the stellar radius to the semimajor axis and the planetary to stellar radius.
3. The orbital period  $P < 3$  days.
4. The planet’s radius  $R_p$  lay between five times Earth’s  $R_{\text{Earth}}$  and 10 times Jupiter’s  $R_{\text{Jupiter}}$ .
5. The planet has an estimated mass  $M_p$ .
6. The planet must have a published orbital period  $P$  and transit midpoint  $T_0$  (called “time of conjunction” in the Exoplanet Archive), along with the corresponding uncertainties.

The disintegrating planet WD 1856+534 b also happens to satisfy all of these criteria, but we dropped it as irrelevant. In some cases, the most recent set of system parameters provided in the Exoplanet Archive did not include required values. In those cases, we used the most recent set of values that did include everything needed. In a handful of cases, we had to calculate the orbital semimajor axes from the provided period and stellar mass. These criteria left us with 137 systems.

### 2.1. Simplified Central Time Uncertainties

To explore the astrophysical properties that support precise transit time estimates, we start with a simplified model for the central time  $t_c$  of a transit or eclipse (Carter et al. 2008). This model involves (among other simplifications) neglecting orbital eccentricity and limb-darkening and assuming that the transiting planet is small compared to the star and that the out-of-transit baseline is very accurately estimated. (Numerical experimentation using fully accurate transit light curves shows that this simplified estimate is good to about 10%.) Carter et al.

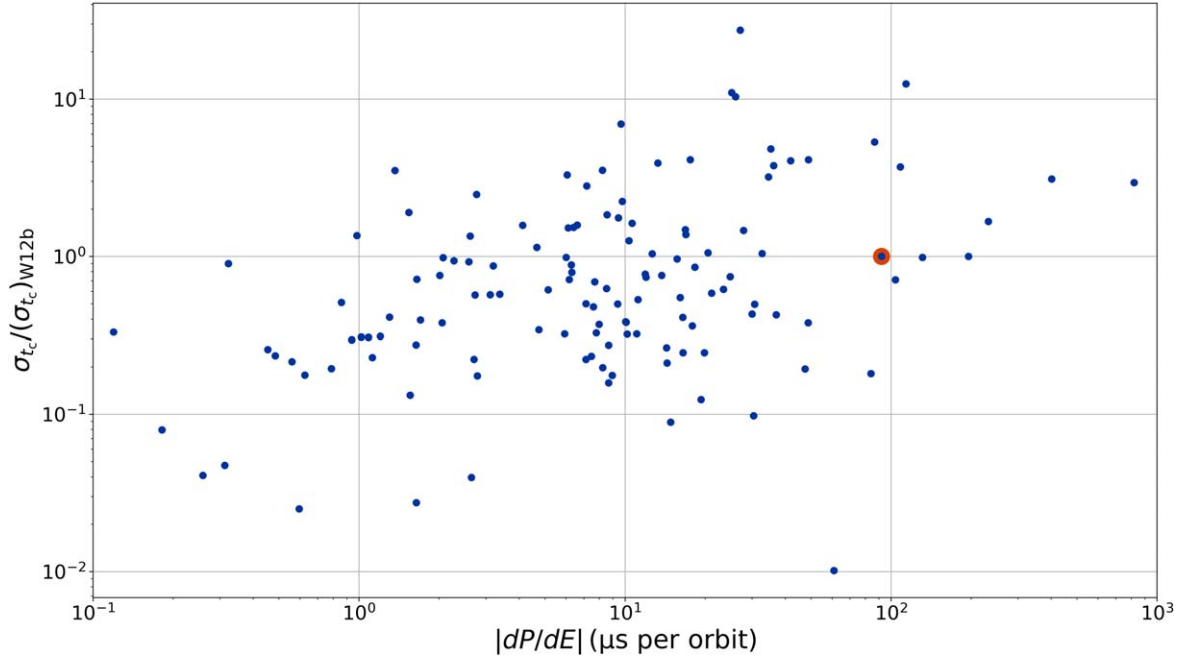


**Figure 1.** Simplified mid-transit time uncertainties (Equation (11)) normalized to the estimate for WASP-12 b (orange marker) vs. the orbital decay (Equation (22) in Section 2.3) for many confirmed systems.

(2008) defined several useful parameters related to the transit:

$$\tau_0 = \frac{R_* P}{a 2\pi}, \quad (3)$$

$$b = \frac{a}{R_*} \cos i, \quad (4)$$

$$T = 2\tau_0 \sqrt{1 - b^2}, \quad (5)$$

$$\tau = 2\tau_0 \left( \frac{R_p}{R_*} \right) (1 - b^2)^{-1/2}, \quad (6)$$

where  $R_*$  is the stellar radius,  $a$  is the orbital semimajor axis,  $P$  is the orbital period,  $i$  is the orbital inclination,  $b$  is the impact parameter,  $T$  is the total transit duration (defined as the time for the planet's center to cross from limb to limb), and  $\tau$  is the ingress/egress duration. We also need a transit or eclipse depth,  $\delta$ ,

$$\delta \approx \begin{cases} \left( \frac{R_p}{R_*} \right)^2 & \text{transit} \\ \left( \frac{R_p}{R_*} \right)^2 \frac{I_p}{I_*} & \text{occultation,} \end{cases} \quad (7)$$

where  $I_{p/*}$  is the planetary/stellar disk-integrated intensity (Winn 2010).

We also need the following parameters as defined in Carter et al. (2008):

$$Q = \sqrt{\Gamma T} \frac{\delta}{\sigma}, \quad (8)$$

$$\theta = \frac{\tau}{T}, \quad (9)$$

where  $\Gamma$  is the sampling rate for the transit observations (assumed constant), and  $\sigma$  is the per-point photometric uncertainty. Therefore,  $Q$  correlates with total signal-to-noise ratio (S/N) for the transit, and  $\theta$  is the ratio of the ingress/

egress duration to the total transit duration. Based on these definitions, Carter et al. (2008) provided a simplified estimate for the uncertainty on the central time  $t_c$ :

$$\sigma_{t_c} = TQ^{-1} \sqrt{\theta/2}. \quad (10)$$

Plugging in all of the above defined parameters, we find that

$$\begin{aligned} \sigma_{t_c} &= \sqrt{\frac{\tau}{2\Gamma}} \left( \frac{\sigma}{\delta} \right) = \sigma \Gamma^{-1/2} \\ &\times \left( \frac{R_*}{a} \right)^{1/2} \left( \frac{P}{2\pi} \right)^{1/2} \left( \frac{R_p}{R_*} \right)^{-3/2} (1 - b^2)^{-1/4} \\ &\times \begin{cases} 1 & \text{transit} \\ \left( \frac{I_p}{I_*} \right)^{-1} & \text{eclipse} \end{cases}. \end{aligned} \quad (11)$$

Not surprisingly, the uncertainty increases with the photometric uncertainty and decreases as the transit depth and sampling rate increase. Why, though, does the mid-transit uncertainty increase with ingress/egress duration? Consider a case with a very long ingress/egress (e.g., a near-grazing transit with  $b \rightarrow 1$ ), which corresponds to a very nearly V-shaped light curve. In that case, determining the mid-transit time relies on being able to determine when exactly the light curve goes from decreasing with time to increasing with time, with very little transition in between. Without sufficient sampling, for example, the instant of transition would be missed, and the mid-transit time would be highly uncertain.

Figure 1 compares estimates of transit  $\sigma_{t_c}$  for several systems to an estimate for WASP-12 b based on Equation (11). Although it is impossible to estimate the per-point photometric uncertainty  $\sigma$  for any system in general, since the photometric uncertainty depends on the complex details of a particular observation, we can at least include the approximate dependence on stellar magnitude. First, we can relate the photon count

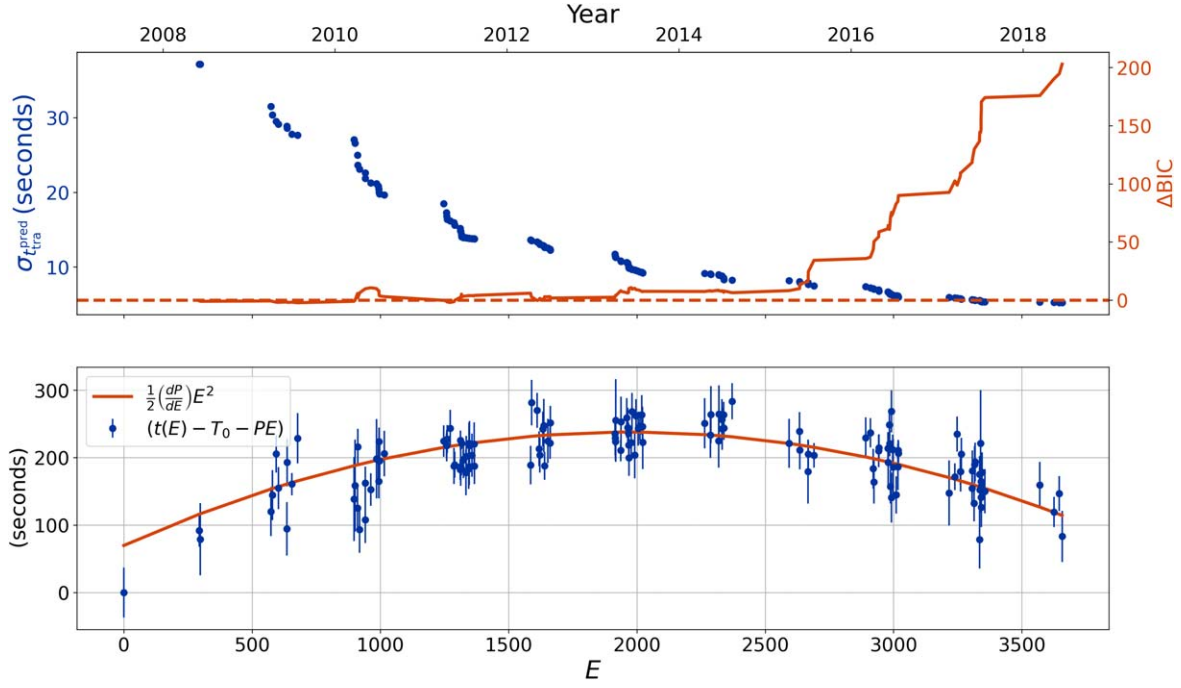


**Figure 2.** (Top) The blue dots show the evolution of  $\sigma_{t_{\text{tra}}}^{\text{pred}}$  for WASP-12 b during the last several years, as calculated using the data from Yee et al. (2020) and Equation (14). The orange curve (which uses the right y-axis) illustrates the corresponding evolution of the difference in BIC comparing a linear ephemeris,  $\text{BIC}(\text{lin})$ , to a quadratic ephemeris,  $\text{BIC}(\text{quad})$ . (Bottom) The blue dots show the difference between the observed transit time  $t(E)$  at epoch  $E$  and a linear ephemeris fit,  $T_0 + PE$ . The orange line shows the quadratic ephemeris term using the  $dP/dE$  ( $-86.7 \mu\text{s orbit}^{-1}$ ) from Yee et al. (2020).

rate  $N$  to the stellar flux in the bandpass of observation  $F$  as  $N \propto F$ . Then we can fold in the relationship between flux and apparent magnitude  $m \propto -2.5 \log_{10} F$ . Assuming Poisson statistics gives

$$\sigma \propto 10^{-m/5}. \quad (12)$$

Although simplified, the calculations illustrated in Figure 1 show that there are many systems that we might expect to have smaller timing uncertainties than WASP-12 b and many systems with tidal decay that are expected to be larger. But there are only three with both: WASP-103 b, KELT-16 b, and KELT-1 b. Barros et al. (2022) analyzed combined ground- and space-based transit observations of WASP-103 b, realizing typical timing uncertainties about 50% smaller than those for WASP-12 b reported in Yee et al. (2020). However, Barros et al. (2022) reported no detection of tidal decay but did see tidal deformation of the planet. Likewise, Harre et al. (2023) combined ground- and space-based data for KELT-16 b and found that the BIC favors no tidal decay, but only slightly:  $\text{BIC} = 292.9$  for a constant period and  $\text{BIC} = 297.6$  for decay. Finally, Baştürk et al. (2023) combined 19 transit observations for the brown dwarf system KELT-1 b and also found no evidence for tidal decay, but they did report possible signs of tidal synchronization of the host star’s rotation.

Having developed a sense for the range of timing uncertainties and tidal decay rates, we next turn to how transit observations are transformed into ephemerides, both those that include no decay (linear in the observational epoch  $E$ ) and those that do include it (quadratic in  $E$ ).

## 2.2. Fitting a Linear Curve to a Linear Ephemeris

For a linear fit to a linear ephemeris based solely on transits, we can calculate the uncertainties on  $T_0$  and  $P$  using the epoch  $E$  for each observed transit and the associated mid-transit time

uncertainty  $\sigma_{t(E)}$ . We use  $\sigma_{t(E)}$  to represent the actually observed uncertainty (as opposed to the analytic uncertainty for a single transit  $\sigma_{t_c}$  or the uncertainty for the predicted future transit time  $\sigma_{t_{\text{tra}}}^{\text{pred}}$ ). The predicted time and associated uncertainty for the transit time are, respectively,

$$t_{\text{tra}}^{\text{pred}} = T_0 + PE, \quad (13)$$

$$\sigma_{t_{\text{tra}}}^{\text{pred}} = \sqrt{\sigma_{T_0}^2 + E^2 \sigma_P^2 + 2E \sigma_{T_0, P}} \approx \sqrt{\sigma_{T_0}^2 + E^2 \sigma_P^2}. \quad (14)$$

Although the  $\sigma_{T_0, P}$  term contributes, in practice, it is usually orders of magnitude smaller than the other terms, so we neglect it.

We can estimate the uncertainties analytically using standard linear regression (see Press et al. 2002). First, define

$$\begin{aligned} S &= \sum_{E \in \text{transits}} (1/\sigma_{t(E)}^2) \\ S_E &= \sum_{E \in \text{transits}} (E/\sigma_{t(E)}^2) \\ S_{E^2} &= \sum_{E \in \text{transits}} (E^2/\sigma_{t(E)}^2). \end{aligned} \quad (15)$$

Then

$$\sigma_{T_0}^2 = \frac{S_{E^2}}{SS_{E^2} - (S_E)^2} \quad (16)$$

$$\sigma_P^2 = \frac{S}{SS_{E^2} - (S_E)^2}. \quad (17)$$

Figure 2 illustrates how adding more and more observations impacts  $\sigma_{t_{\text{tra}}}^{\text{pred}}$  by following the history of transit observations of WASP-12 b.

Of course, if we wait for a while before observing another transit, the uncertainty for the next expected transit time will

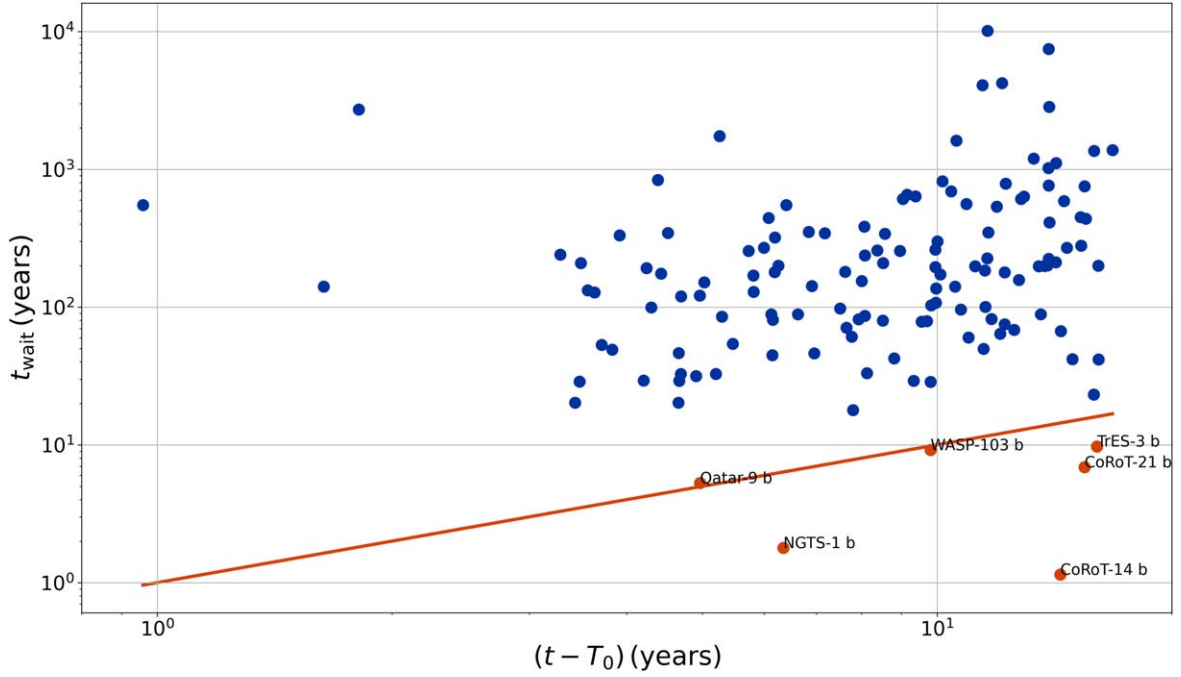


**Figure 3.** Time  $t_{\text{wait}}$  expected before the uncertainty on the linear ephemeris  $\sigma_{t_{\text{tra}}^{\text{pred}}}$  (Equation (14)) grows as large as the transit duration  $T$  vs. the time (as of 2023 April 5) since the  $T_0$  value reported in the Exoplanet Archive. The orange line shows  $y = x$ , and the orange points are systems that lie near or below that line. For these systems, additional transit observations would likely significantly improve the linear ephemeris.

grow as in Equation (14). If we waited long enough,  $t_{\text{wait}}$ , that  $\sigma_{t_{\text{tra}}^{\text{pred}}}$  grows beyond some value, then scheduling the next transit observation could be challenging:

$$t_{\text{wait}} = \sqrt{\sigma_{t_{\text{tra}}^{\text{pred}}}^2 - \sigma_{T_0}^2} \left( \frac{P}{\sigma_P} \right). \quad (18)$$

Systems that have not been observed for  $t_{\text{wait}}$  are the ones for which additional transit observations would be most fruitful for improving the linear ephemeris. For the systems considered here, Figure 3 shows the expected time we would have to wait for  $\sigma_{t_{\text{tra}}^{\text{pred}}}$  to grow as large as the transit duration  $T$  since the  $T_0$  value reported in the Exoplanet Archive (as of 2023 April 5). Most planets have sufficiently precise linear ephemerides that we would have to wait many years before the uncertainties on their expected  $t_{\text{tra}}^{\text{pred}}$  grew as large as their transit durations, but uncertainties for a handful are likely large enough to warrant follow-up already, at least based on the Exoplanet Archive data. For example, CoRoT-14 b has an orbital period  $P = 1.51214 \pm 0.00013$  days and  $T_0 = 2,454,787.6702 \pm 0.0053$  JD (Bonomo et al. 2017), which corresponds to 2008 November. Over the last decade and a half,  $\sigma_{t_{\text{tra}}^{\text{pred}}}$  has grown as large as its transit duration,  $T = 1.2$  hr. Very near the one-to-one line, WASP-103 b was recently observed by the CHEOPS telescope, observations that actually suggest an orbital period increase rather than a decrease (Barros et al. 2022). However, the resulting ephemeris was too recent to have been included in our data, so we do not consider it here. A similar case is TrES-3 b; we did not use more recent observations (e.g., Mannaday et al. 2022) that would likely update its timing uncertainty and increase  $t_{\text{wait}}$ . Determining whether individual systems require follow-up or just updated ephemerides is left for future work.

Finally, fitting a linear curve to a linear ephemeris would be expected to result in a BIC given by

$$\text{BIC}(\text{lin}) = (N - 2) + 2 \ln N. \quad (19)$$

### 2.3. Fitting a Quadratic Curve to a Quadratic Ephemeris

For a quadratic ephemeris, the predicted time and associated uncertainty for the time of the  $E$ th transit are, respectively,

$$t_{\text{tra}}^{\text{pred}} = T_0 + PE + \frac{1}{2} \left( \frac{dP}{dE} \right) E^2, \quad (20)$$

$$\sigma_{t_{\text{tra}}^{\text{pred}}} \approx \sqrt{\sigma_{T_0}^2 + E^2 \sigma_P^2 + \frac{1}{4} E^4 \sigma_{dP/dE}^2}, \quad (21)$$

where we have again neglected covariance between fit parameters.

For tidal decay involving a constant phase lag (i.e., a constant value for the star's modified tidal dissipation parameter  $Q_*$ ),  $dP/dE$  is given by

$$\begin{aligned} \frac{dP}{dE} &= P \frac{dP}{dt} \approx -(26 \mu\text{s per orbit}) \\ &\times \left( \frac{M_p}{M_{\text{Jup}}} \right) \left( \frac{M_*}{M_\odot} \right)^{-8/3} \left( \frac{R_*}{R_\odot} \right)^5 \\ &\times \left( \frac{P}{\text{day}} \right)^{-10/3} \left( \frac{Q_*}{10^5} \right)^{-1}, \end{aligned} \quad (22)$$

where  $M_p$  is the planetary mass in Jupiter masses ( $M_{\text{Jup}} = 1.89813 \times 10^{27}$  kg),  $M_*$  is the stellar mass in solar masses ( $M_\odot = 1.989 \times 10^{30}$  kg),  $R_*$  is the stellar radius in solar radii ( $R_\odot = 6.957 \times 10^8$  m), and  $P$  is the orbital period in days.

Figure 1 compares estimates of  $dP/dE$  for many systems to  $dP/dE$  for WASP-12, assuming a WASP-12-like

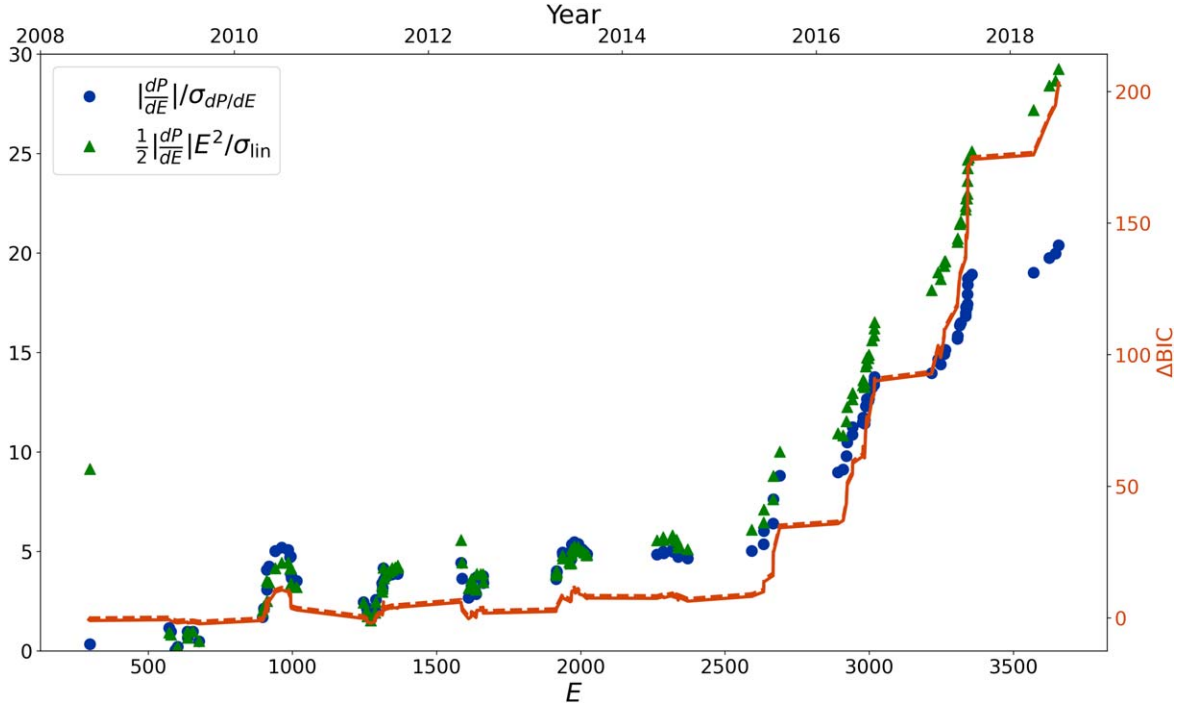


**Figure 4.** The blue dots show the evolution of the tidal decay  $S/N = \left| \frac{dP}{dE} \right| / \sigma_{dP/dE}$  for WASP-12. The green triangles show the corresponding evolution of the best-fit quadratic term  $\frac{1}{2} \left| \frac{dP}{dE} \right| E^2 / \sigma_{\text{lin}}$ . Both of these data use the left y-axis. The orange curve shows the same difference in BIC values as shown in Figure 2 calculated numerically. These results are based on the same data as in Figure 2 and reported in Yee et al. (2020). The dashed orange line shows the analytic approximation given by Equation (35).

$Q_* = 2 \times 10^5$ . Interestingly, many systems might be expected to exhibit faster tidal decay, and many more systems likely have properties that give rise to more precise transit timing  $\sigma_{t_c}$ , at least based on the simplified analytic treatment outlined in Section 2.1.

By analogy with the linear case, we can analytically calculate the uncertainties on the fit parameters. For this calculation, we define

$$\begin{aligned} S_{E^3} &= \sum_{E \in \text{transits}} (E^3 / \sigma_{t(E)}^2), \\ S_{E^4} &= \sum_{E \in \text{transits}} (E^4 / \sigma_{t(E)}^2). \end{aligned} \quad (23)$$

With these definitions,

$$\sigma_{T_0}^2 = \frac{S_{E^3}^2 - S_{E^2} S_{E^4}}{\Delta}, \quad (24)$$

$$\sigma_P^2 = \frac{S_{E^2}^2 - S S_{E^4}}{\Delta}, \quad (25)$$

$$\sigma_{dP/dE}^2 = \frac{S_E^2 - S S_{E^2}}{\Delta}, \quad (26)$$

where

$$\Delta = -S S_{E^2} S_{E^4} + S S_{E^3}^2 + S_E^2 S_{E^4} - 2 S_E S_{E^2} S_{E^3} + S_{E^2}^3. \quad (27)$$

Fitting a quadratic curve to a quadratic ephemeris would be expected to result in

$$\text{BIC}(\text{quad}) = (N - 3) + 3 \ln N. \quad (28)$$

We can use these expressions to explore how evidence for tidal decay in the WASP-12 system mounted over the years as

a template for finding other systems exhibiting tidal decay. The blue dots in Figure 4 shows the evolution of the tidal decay  $S/N$  for WASP-12 b alongside the comparison of the BIC for linear and quadratic fits,  $\Delta\text{BIC} \equiv \text{BIC}(\text{lin}) - \text{BIC}(\text{quad})$ . The  $\Delta\text{BIC}$  will grow as the data favor tidal decay. Not surprisingly, as the tidal decay  $S/N$  goes up, the BIC preference for the quadratic fit increases, too.

Another requirement for the observational constraints on  $dP/dE$  to be meaningful is that uncertainties on the linear portion of the ephemeris need to be small compared to the quadratic portion. Otherwise, apparent deviations from a putative linear ephemeris due to tidal decay could be attributed to the uncertainties on the linear ephemeris. This condition translates to

$$\sigma_{\text{lin}} \equiv \sqrt{\sigma_{T_0}^2 + E^2 \sigma_P^2} < \frac{1}{2} \left| \frac{dP}{dE} \right| E^2. \quad (29)$$

Figure 4 shows how this condition played out for WASP-12 b. The increase in  $\Delta\text{BIC}$  clearly correlates with the growth of the quadratic term in Equation (29).

Considering other systems, Figure 5 shows the cumulative change in orbital period expected due to tidal decay for our collection of systems as compared to the uncertainty on the linear ephemeris. Systems satisfying Equation (29) appear above the orange line. For example, WASP-12, the only system for which tidal decay has been definitively observed, appears above that line, along with several other systems. Several caveats should be considered in evaluating these results, including the fact that we have assumed  $Q_* = 2 \times 10^5$ . This is the value inferred for WASP-12, which may exhibit unusually efficient tidal dissipation (Weinberg et al. 2017) and therefore may not be a representative value. For some well-observed systems, such as

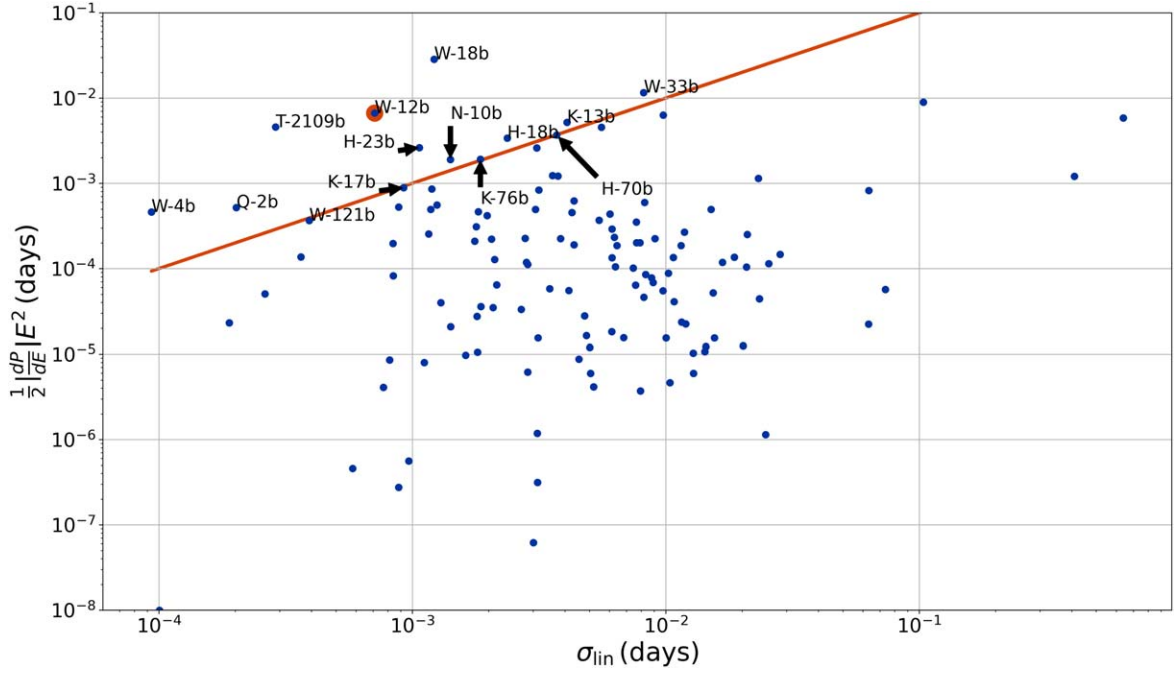


**Figure 5.** Cumulative change in orbital period due to tidal decay expected theoretically vs. uncertainties on the linear ephemeris (Equation (14)). WASP-12 b is shown with an orange circle, and the orange line shows  $y = x$ . Systems above that line may have experienced sufficient tidal decay since  $T_0$  that it is distinguishable from the uncertainties on the linear ephemeris. Individual planets near or above the line are labeled as follows: HAT-P-23 b = “H-23b,” HATS-18 b = “H-18b,” HATS-70 b = “H-70b,” KOI-13 b = “K-13b,” Kepler-17 b = “K-17b,” Kepler-76 b = “K-76b,” NGTS-10 b = “N-10b,” Qatar-2 b = “Q-2b,” TOI-2109 b = “T-2109b,” WASP-12 b = “W-12b,” WASP-121 b = “W-121b,” WASP-18 b = “W-18b,” WASP-33 b = “W-33b,” and WASP-4 b = “W-4b.”

WASP-18b and WASP-19b, the lack of observed orbital decay to date has been used to constrain their values of  $Q_*$  to  $>10^7$  and  $>10^6$ , respectively (Rosário et al. 2022). Even so, the results point to several systems that merit follow-up transit observations. Several of the systems above the line in Figure 5 have been noted to exhibit period changes. For example, HAT-P-23 has  $\frac{1}{2} \left( \frac{dP}{dE} \right) E^2 = -0.003$  and  $\sigma_{lin} = 0.002$  days, while Hagey et al. (2022) reported  $dP/dt = -5.2 \pm 5.8 \text{ ms yr}^{-1}$  (which works out to  $\Delta P \approx -0.004$  days since  $T_0$  for HAT-P-23 b).

#### 2.4. Fitting a Linear Curve to a Quadratic Ephemeris

Finally, we consider the case of fitting a linear curve to a quadratic ephemeris. Analyzing this case is useful because it will allow us to explore how to estimate the BIC thresholds we should look for if we suspect a planet shows signs of tidal decay. (The other combination, fitting a quadratic to a linear ephemeris, would, in principle, result in a quadratic coefficient statistically consistent with zero and the same BIC expression as in Section 2.3.)

To start, consider the linear curve that results from fitting the quadratic ephemeris. Since  $|dP/dE| \ll T_0$  and  $\ll P$  (where  $T_0$  and  $P$  are the true values for the system), we might suspect that the best-fit values, which we will call  $T'_0$  and  $P'$ , would closely resemble the actual values, i.e.,  $T'_0 \approx T_0$  and  $P' \approx P$ . Indeed, fitting a linear curve to the transit times for WASP-12 b from Yee et al. (2020) returns  $T'_0$  and  $P'$  that match  $T_0$  and  $P$  to better than a few parts in 10,000. But the large collection of high-quality data for WASP-12 b means that even this small disagreement is still statistically discrepant. This result comports with the results from Section 2.3; those systems for which we have sufficient data to detect a nonzero  $dP/dE$  are also those for which we have very small error bars on  $T_0$  and  $P$ . Therefore, in order to calculate the BIC for fitting a linear curve

to a quadratic ephemeris, we will need to also calculate  $T'_0$  and  $P'$ , which can be written as

$$T'_0 = T_0 + \left( \frac{dP}{dE} \right) \Delta T'_0, \quad (30)$$

$$P' = P + \left( \frac{dP}{dE} \right) \Delta P', \quad (31)$$

where  $\Delta T'_0$  and  $\Delta P'$  are the corrections we need to work out. As outlined in the Appendix, standard linear regression gives the following formulae for  $\Delta T'_0$  and  $\Delta P'$ :

$$\Delta T'_0 = \left( \frac{S_E^2 - S_E^3 S_E}{S_E^2 S - S_E^2} \right), \quad (32)$$

$$\Delta P' = \left( \frac{S_E^3 S - S_E^2 S_E}{S_E^2 S - S_E^2} \right). \quad (33)$$

Now we can calculate the resulting  $\chi^2$  for fitting a linear curve to a quadratic ephemeris,

$$\begin{aligned} \chi^2 &= \sum_{E \in \text{transits}} \left( \frac{t(E) - P'E - T'_0}{\sigma_{t(E)}} \right)^2 \\ &\approx \frac{1}{4} \left( \frac{dP}{dE} \right)^2 \sum_{E \in \text{transits}} \left( \frac{E^2 - \Delta P'E - \Delta T'_0}{\sigma_{t(E)}} \right)^2 + (N - 2), \end{aligned} \quad (34)$$

and the difference in BIC values for a linear curve and a quadratic curve, both fit to a quadratic ephemeris as determined

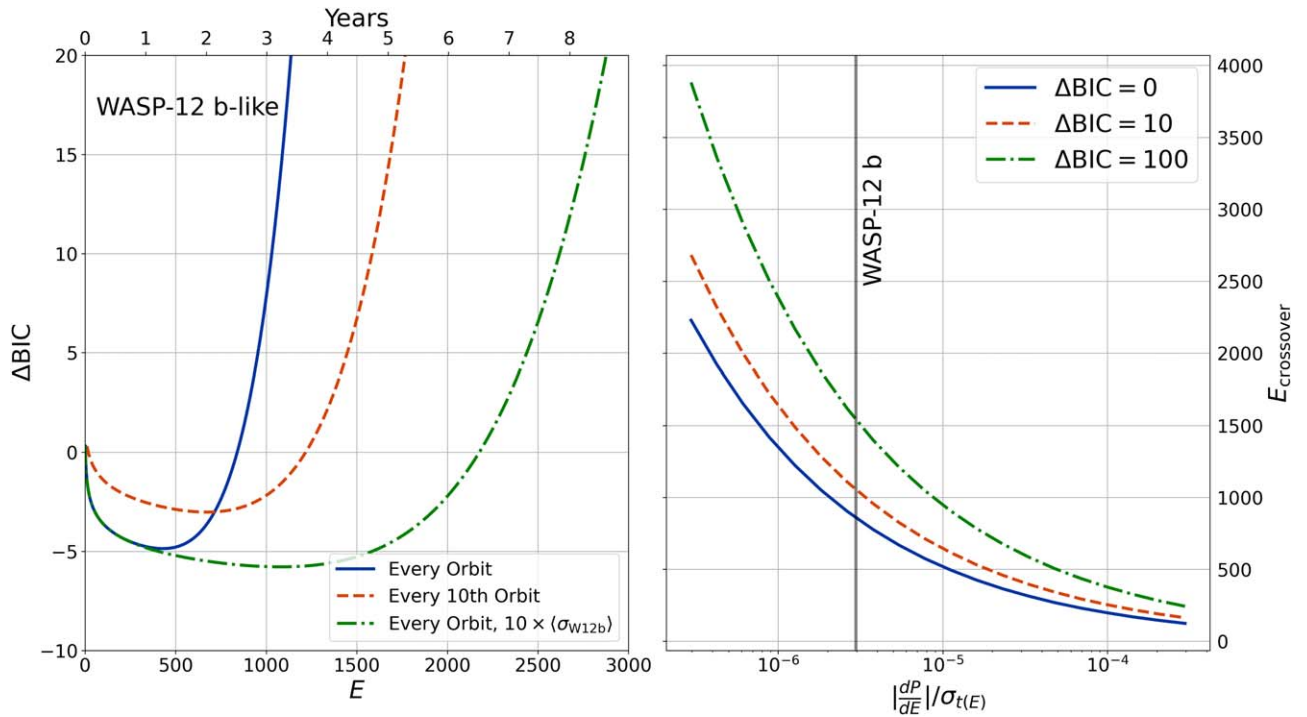


**Figure 6.** Application of Equation (35) to planetary systems with WASP-12 b-like tidal decay and transit timing uncertainties. The left panel shows the evolution of  $\Delta\text{BIC}$  assuming that a transit is observed (1) every orbit (solid blue), (2) every 10th orbit (dashed orange), and (3) every orbit but with a timing uncertainty that is 10 times larger than the other two cases (dashed-dotted green). The right panel shows the epoch  $E_{\text{crossover}}$  at which  $\Delta\text{BIC}$  crosses over a given value as a function of the tidal decay rate ( $dP/dE$ ) and transit timing uncertainty  $\sigma_{t(E)}$ . As a point of comparison, for WASP-12 b,  $|dP/dE|/\sigma_{t(E)} \approx 3 \times 10^{-6}$ , as shown by the vertical gray line. These curves optimistically assume that the transit for every epoch is observed up to  $E_{\text{crossover}}$ .

analytically:

$$\Delta\text{BIC} = \frac{1}{4} \left( \frac{dP}{dE} \right)^2 \sum_{E \in \text{transits}} \left( \frac{E^2 - \Delta P'E - \Delta T'_0}{\sigma_{t(E)}} \right)^2 - \ln N + 1. \quad (35)$$

Of course, given a set of already observed transits, we could easily calculate the  $\Delta\text{BIC}$ . The benefit of Equation (35) is that we can estimate the  $\Delta\text{BIC}$  expected for a sequence of planned transit observations that have yet to be conducted (given reasonable estimates for the expected timing uncertainties). The dashed orange line in Figure 4 shows how closely the analytic approximation matches the numerical result obtained by directly comparing a linear to a quadratic fit.

### 3. Applying the $\Delta\text{BIC}$ Expression

Applying Equation (35) to the ephemerides for transiting planets can provide the likelihood of detecting tidal decay for a given planned series of transit campaigns; for an expected tidal decay rate (Equation (22)), when should observations be collected, and how many? A comprehensive application of Equation (35) to the suite of transiting hot Jupiters could be fruitful in these ways, but for the present paper, we confine our application to a few example cases.

#### 3.1. Hypothetical Cases

First, we consider hypothetical cases to gauge how effectively tidal decay could, in principle, be detected by various observing strategies for planetary systems with definite quadratic ephemerides. For many of the calculations in this section, we assumed a tidal decay rate equal to WASP-12 b's,

$P/|dP/dt| = 2.3 \text{ Myr}$  or  $dP/dE = 86.7 \mu\text{s orbit}^{-1}$  (Yee et al. 2020), and a constant transit timing uncertainty,  $\sigma_{t(E)} = \text{const}$ . Strictly,  $\Delta\text{BIC}$  depends on the transit epoch  $E$  and not on orbital period, but to give a sense of the timescales over which observational campaigns might be conducted, we assumed WASP-12 b's orbital period  $P = 1.091419649$  days to convert from  $E$  to years.

To begin with, we consider some overly simple observational campaigns (left panel of Figure 6). (N.B.: Throughout this section, the  $x$ - and  $y$ -axes of different panels often do not match up.) For the blue and orange lines, that uncertainty was taken as equal to the median for the WASP-12 b data set from Yee et al. (2020),  $\sigma_{t(E)} = \langle \sigma_{W12b} \rangle = 0.00032$  days, while the green line shows the result for an uncertainty that is 10 times larger (0.0032 days). The blue and green lines show how  $\Delta\text{BIC}$  would grow if we could (unrealistically) observe every transit, while the orange line shows what would happen if we observed every 10th transit.

As previously stated,  $\Delta\text{BIC} > 0$  indicates a statistical preference for a quadratic over a linear ephemeris, and all curves in the left panel of Figure 6 show  $\Delta\text{BIC}$  initially dropping from zero into negative values. Intuitively, this behavior reflects the need for curvature in the ephemeris to build up over time so that the quadratic term ( $\frac{1}{2}|dP/dE|E^2$ ; see Equation (20)) grows sufficiently large that a linear regression is impacted. In other words, we have to wait for a while after a transiting planet is discovered to spot tidal decay. Equation (35) indicates that that crossover point depends on the total number of observations  $N$ , the timing/frequency of those observations (the summation term), the timing uncertainty, and the tidal decay rate  $dP/dE$ .



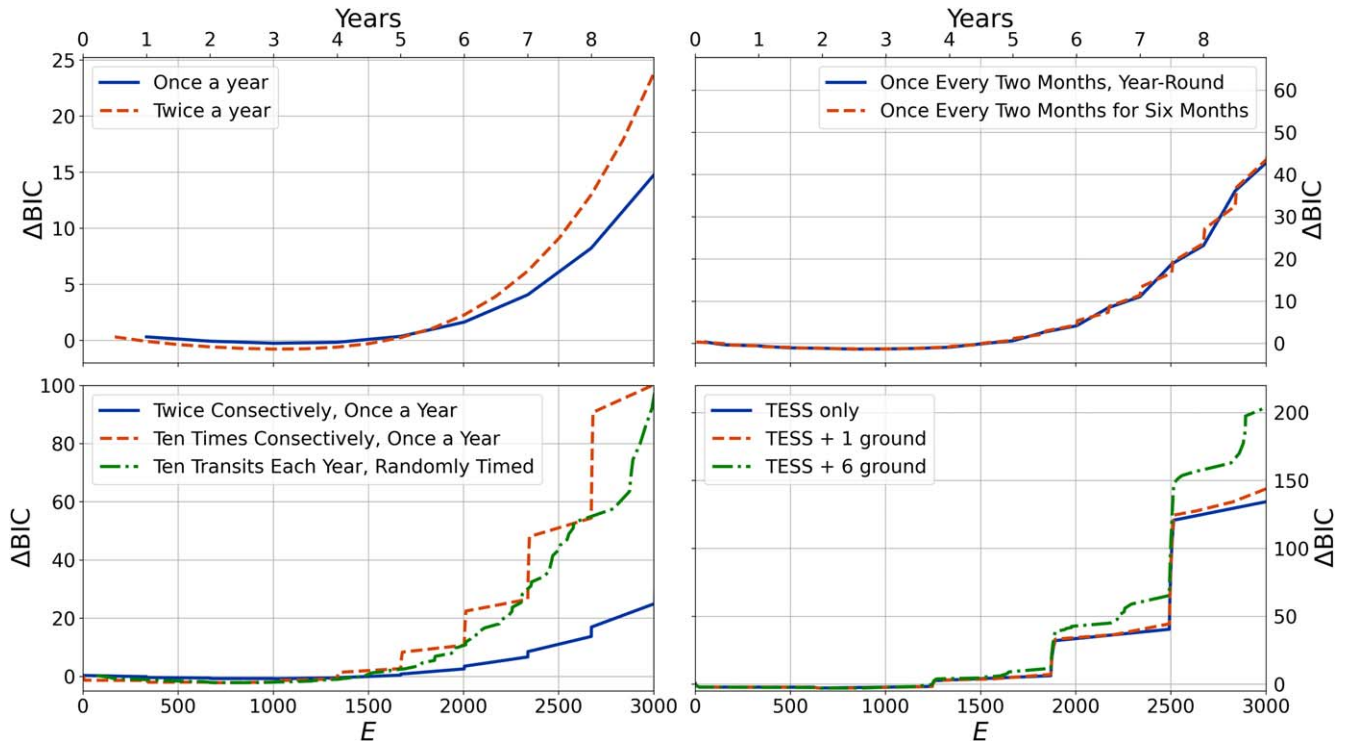


**Figure 7.** Application of Equation (35) to planetary systems with WASP-12 b-like tidal decay and transit timing uncertainties using more realistic observing strategies. The top left panel shows how  $\Delta\text{BIC}$  grows with one or two transit observations in an Earth year. The top right panel shows how  $\Delta\text{BIC}$  grows with bimonthly transit observations during a whole (Earth) year (solid blue curve) and during a hypothetical observing season of 6 months with no observations during the other 6 months. The bottom left panel shows how  $\Delta\text{BIC}$  grows assuming two consecutive transit observations each Earth year (solid blue curve) and 10 consecutive observations each Earth year (dashed orange curve). The dashed-dotted green curve shows the same total number of transits (10 annually) as the dashed orange curve but randomly timed. The bottom right panel shows how  $\Delta\text{BIC}$  evolves for an observational program meant to mimic TESS observations (“TESS only”; solid blue). That program involves about two dozen transits once every 25 TESS sectors, which span 27 days each. The dashed orange line (“TESS + ground”) shows the same observing program but with the addition of one transit observation every 6 months, meant to represent a ground-based observation. Observations for both programs assume the same transit timing uncertainties.

The right panel of Figure 6 shows the dependence of the crossover epoch  $E_{\text{crossover}}$  for a desired  $\Delta\text{BIC}$  value on the ratio  $|dP/dE|/\sigma_{\tau(E)}$ , assuming that every transit since a planet’s discovery is observed. If, for example,  $\Delta\text{BIC} = 10$  were the goal of an observing program (dashed orange curve) for a system with WASP-12 b-like properties ( $|dP/dE|/\sigma_{\tau(E)} \approx 3 \times 10^{-6}$ ), then a minimum of about 1000 transits would need to be observed. Approaching the situation from the opposite direction, a survey including nearly every single transit up to  $E = 1500$  and with WASP-12 b-like timing uncertainties would be expected to achieve  $\Delta\text{BIC} \approx 100$  if the system actually exhibited WASP-12 b’s tidal decay. In this way, we can apply Equation (35) to a particular observing program to determine a reasonable threshold for decay detection.

Next, we consider somewhat more realistic observing campaigns (Figure 7). The top left panel compares  $\Delta\text{BIC}$  growth for one transit observation and two observations in 1 Earth yr. In about 9 Earth yr, the curve corresponding to twice-annual observations (dashed orange) has grown to nearly twice the  $\Delta\text{BIC}$  for once-annual observations (solid blue). The top right panel compares  $\Delta\text{BIC}$  growth for one observation every 2 months all Earth year-round and the other involving one observation every 2 months for 6 months (dashed orange). Here the two curves weave over one another, suggesting little advantage of one program over the other. This result is not surprising, since little curvature develops in the ephemeris over 6 months.

Next, consider the bottom left panel of Figure 7. The solid blue curve involves two consecutive transit observations each

Earth year, while the dashed orange curve involves 10 consecutive observations each Earth year. Not surprisingly,  $\Delta\text{BIC}$  increases much more rapidly for the latter program than the former because, in each observing session, significantly more transits are collected. The dashed-dotted green curve involves the same total number of transits as the dashed orange curve but randomly phased (i.e., not necessarily consecutive transits), illustrating that the timing of observations over a short (compared to the decay time) timescale has minimal impact on the evolution. For this particular instantiation, the final  $\Delta\text{BIC}$  ends up slightly below the dashed orange curve, but other examples (not shown) have  $\Delta\text{BIC}$  equal to or even slightly above the dashed orange curve, depending on exactly how the observations are timed.

Finally, consider the bottom right panel of Figure 7. This panel shows how ground-based observations can combine with observations from a TESS-like mission to detect tidal decay. For this calculation, we first assumed that every transit was observed for a WASP-12-like system during a 27 day period in each year, followed by no observations for 25 TESS sectors, and then another sequence of transits were observed, etc. The solid blue line shows this scenario. The dashed orange line shows the same program except with a single ground-based transit included every 6 months. The dashed-dotted green line shows the same program except with six ground-based transit observations randomly spread out during a 6 month observing season. Not surprisingly, the  $\Delta\text{BIC}$  for the TESS + ground programs grows more quickly, demonstrating the power of

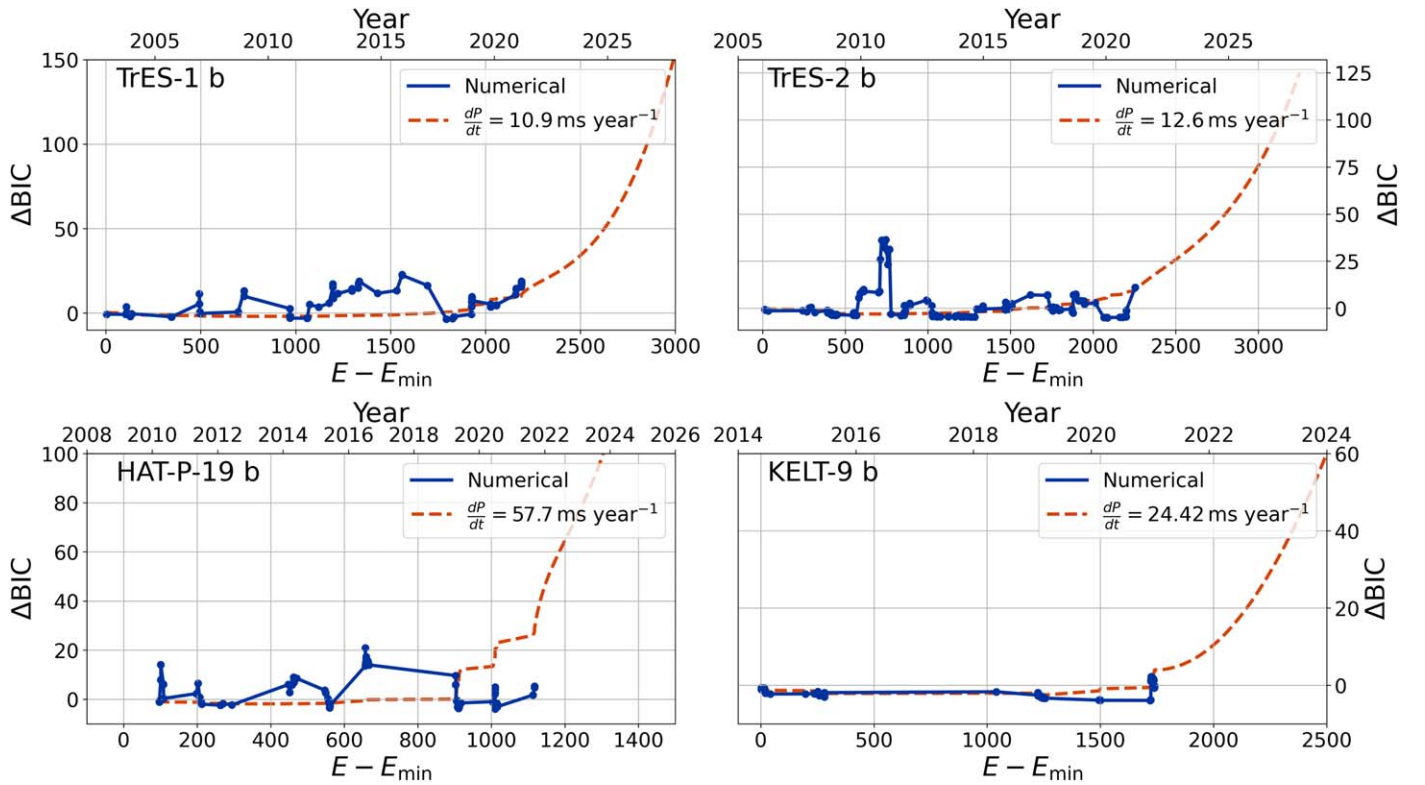


**Figure 8.** Evolution of  $\Delta\text{BIC}$  for several real planets. The solid blue “Numerical” lines show the evolution based on previously published observations, while the dashed orange lines show the evolution based on Equation (35). For points in the latter calculation beyond the previously published observations, we assumed  $\sigma_{\pi(E)}$  equal to the average uncertainty for the previously published observations. We also assumed the transits were observed at a cadence equal to the median cadence for the previously published observations. For example, previous transit observations of TrES-2 b have typically been conducted once every four orbits. Observations for TrES-1 b, TrES-2 b, and HAT-P-19 b come from Hagey et al. (2022), and observations for KELT-9 b come from Harre et al. (2023). For this plot, we have subtracted the minimum reported epoch  $E_{\min}$  from  $E$ .

combining the two approaches. The dashed-dotted green line (six ground-based transits) significantly exceeds the solid blue line once the signal of tidal decay starts to emerge and  $\Delta\text{BIC}$  grows large, while the dotted orange line (one ground-based transit) only modestly exceeds it.

Although the approach here needs to be tailored to each specific observing program for detailed predictions, these results illustrate its general utility. They show that detecting tidal decay requires collecting regular observations and allowing sufficient time for decay to manifest. In general, a significant increase in  $\Delta\text{BIC}$  requires a significant fractional increase in the number of observations. Adding just a few more observations to an already full observing program does not make much difference unless they are judiciously timed. Two encouraging conclusions of these results: (1) an observing program that can only observe a few times a year can still have an impact, and (2) it may be more worthwhile to double the number of candidates, focusing on the planets most likely to exhibit decay, than to double the number of transits observed for a given planet if a program already involves several observations in a year.

### 3.2. Real Cases

Finally, we consider real systems (Figure 8). These examples all involve systems for which possible tidal decay has been reported. We take observations for TrES-1 b, TrES-2 b, and HAT-P-19 b from Hagey et al. (2022) and KELT-9 b from Harre et al. (2023). For the calculations in this section, we take the correct (and variable) transit timing uncertainties and the

corresponding orbital periods to convert epoch  $E$  to (Earth) years. To extrapolate the  $\Delta\text{BIC}$  evolution forward in time, we assume that observations continue with the same median frequency as before. For example, TrES-2 b has been observed every four orbits, so we assume that same observing cadence going on past 2020.

Hagey et al. (2022) analyzed transit times reported in the Exoplanet Transit Database,<sup>3</sup> and, for TrES-1 b, a tidal decay rate  $dP/dt = -10.9 \pm 2.1 \text{ ms yr}^{-1}$  was favored over a constant period by  $\Delta\text{BIC} = 9.7$ . The left panel of Figure 8 shows a good match between the numerical and analytic estimates for  $\Delta\text{BIC}$ , and, assuming the nominal tidal decay rate, the analytic estimate suggests that  $\Delta\text{BIC}$  ought to exceed 50 within the next few years. However, it may take until about 2030 to reach the same level as reported for WASP-12 b in Yee et al. (2020); not surprising, given that WASP-12 b’s  $dP/dt$  is about twice as large.

Moving next to TrES-2 b, Hagey et al. (2022) estimated  $dP/dt = -12.6 \pm 2.4 \text{ ms yr}^{-1}$  with tidal decay favored at  $\Delta\text{BIC} = 8.3$ . Again, Figure 8 shows a good match between the numerical and analytic estimates (albeit with considerable scatter in the “Numerical” estimate). Again, the smaller  $dP/dt$  than WASP-12 b’s means that  $\Delta\text{BIC}$  grows more slowly and may not exceed 50 until 2025. Like the TrES-1 data, the TrES-2 observational data show significant statistical fluctuations in  $\Delta\text{BIC}$ ; between  $E - E_{\min} = 500$  and 1000,  $\Delta\text{BIC}$  climbed rapidly before settling back toward zero. The dashed orange

<sup>3</sup> <http://var2.astro.cz/ETD/>

line shows that such a rapid increase would not have been expected so soon after the planet’s discovery. It remains to be seen whether the recent upward tick in  $\Delta\text{BIC}$  seen in the most recent data represents the beginning of a true increase or whether it too is another statistical fluctuation, although the upward tick is consistent with expectations.

For HAT-P-19 b, Hagey et al. (2022) reported  $dP/dt = -55.2 \pm 7.2 \text{ ms yr}^{-1}$  and  $dP/dE = 606 \mu\text{s orbit}^{-1}$ , with tidal decay favored at  $\Delta\text{BIC} = 8.3$ . This  $dP/dE$  value is almost seven times that for WASP-12 b, and the analytic  $\Delta\text{BIC}$  reflects this, with a value predicted to exceed that for WASP-12 b by 2024. However, the “Numerical” estimate shows considerable nonmonotonicity, reversing direction and sign several times during the observational baseline. The “Numerical”  $\Delta\text{BIC}$  appears to significantly underperform the analytic estimate. In this context, the right panel of Figure 6 is particularly useful. The average timing uncertainty for the HAT-P-19 b data is 0.0007296 days, about twice the average for WASP-12 b (0.00032 days). If all orbits since discovery had been observed, by  $E - E_{\min} = 1000$ , we would expect  $\Delta\text{BIC}$  to exceed 100 (dashed-dotted green line in the right panel of Figure 6). Of course, not every orbit of HAT-P-19 b has been observed, but the fact that the “Numerical”  $\Delta\text{BIC}$  does not yet exceed 10 suggests that perhaps the tidal decay reported for HAT-P-19 b is spurious.

Finally, Harre et al. (2023) combined ground-based, Spitzer, TESS, and CHEOPS transits and eclipses of the ultrahot Jupiter KELT-9 b, which orbits a star at the A/B stellar type boundary, and reported a possible decay rate of  $dP/dt = -24.42 \pm 10.66 \text{ ms yr}^{-1}$  with  $\Delta\text{BIC} = 8.4$  (although the data show a preference,  $\Delta\text{BIC} = 13.2$ , for apsidal precession). Figure 8 shows that the “Numerical”  $\Delta\text{BIC}$  only became positive with the most recent observations before nosing back to zero with the very last observation. The analytic curve suggests that  $\Delta\text{BIC}$  would not have been expected to cross zero until recently anyway and that it might surpass 20 in 2023. Ivshina & Winn (2022) also considered TESS observations of KELT-9 b and found no evidence for decay. Continued monitoring, especially observations of planetary eclipses, seems likely to resolve whether the system actually experiences tidal decay, which would be especially surprising, since A/B stars are not expected to exhibit significant tidal dissipation (Ogilvie 2014).

What to make of all of these comparisons? One key conclusion is that statistical fluctuations in  $\Delta\text{BIC}$  often appear and may falsely hint at tidal decay. Continued, sustained growth in  $\Delta\text{BIC}$  is probably required to confidently report detection of tidal decay. A calculation like that depicted in the right panel of Figure 6 tailored for a specific campaign provides a way of assessing the threshold  $\Delta\text{BIC}$  beyond which tidal decay may be plausible.

#### 4. Discussion and Conclusions

The approach presented here allows observers to plan observational programs to maximize the possibility for detecting tidal decay while minimizing the required resources. This approach is framed in such a way that it does not, in principle, even require observations to make useful predictions; if observers have estimates for the expected transit timing uncertainty (Equation (11)) and tidal decay rate (Equation (22)), along with a planned observational sequence

(which orbital epochs will be observed), Equation (35) provides a way of estimating the likelihood of detecting tidal decay.

Naturally, this approach comes with important caveats and limitations. For instance, we have assumed a linear regression approach, but real transit data may have complex and asymmetric uncertainties (Hagey et al. 2022) for which such an approach is only an approximation. Our approach also assumes that the BIC provides an accurate means for comparing models with tidal decay and those without. However, the BIC is only valid for sample sizes much larger than the number of model parameters (Schwarz 1978). Fortunately, seeking signs of tidal decay necessitates a large number of observations, so this requirement is likely always fulfilled in this context. Finally, we have limited our scope to tidal decay and have not explicitly considered other astrophysical processes that can affect the ephemeris. But our approach should apply to any mechanism that introduces a quadratic term into the ephemeris, so it should be able to capture the impact of precession on both transit and eclipse timings (Winn 2010). Our method can likely be extended to consider other simple ephemeris effects, as long as they can be readily captured by a linear regression approach.

Another potentially fruitful extension would be to incorporate a more sophisticated relationship between stellar properties and tidal decay rate. Studies of stellar tides suggest that the deeper convective zones in later-type (i.e., cooler) stars tend to promote tidal dissipation, resulting in smaller tidal dissipation parameters  $Q_*$  (e.g., Barker 2022), which would tend to recommend their planetary systems as good targets for detecting tidal decay. Main-sequence, cooler stars tend to be smaller, too, giving deeper transits and therefore smaller timing uncertainties (Equation (11)). On the other hand, main-sequence cooler stars are dimmer, which tends to inflate the photometric uncertainty (Equation (12)). Figuring out how to thread this needle and choose the best set of stars to optimize decay detection should be the subject of future work.

As discussed in Section 1, detecting tidal decay is critical for constraining  $Q_*$  and planetary engulfment rates. As pointed out in Metzger et al. (2012), the engulfment rate should scale roughly as  $Q_*$ , and if many stars had  $Q_*$  values as small as WASP-12’s, we might expect a galactic engulfment rate as large as  $18 \text{ yr}^{-1}$ . This value is likely overly large, since there is reason to believe WASP-12 has unusually dissipative tides (Bailey & Goodman 2019). Determining the actual rate is important for future surveys for engulfment signatures because the larger the rate, the fewer stars would need to be monitored to catch engulfment. By efficiently directing searches for tidal decay, the approach outlined here would feed forward to guide surveys to search for engulfment as well.

#### Acknowledgments

We acknowledge useful feedback from an anonymous referee. This study was supported by a grant from NASA’s Exoplanet Research Program.

*Software:* astropy (Astropy Collaboration et al. 2013, 2018), matplotlib (Hunter 2007), numpy (Harris et al. 2020), scipy (Virtanen et al. 2020).

## Appendix

We start with an ephemeris that resembles Equation (20),

$$t(E) = T_0 + PE + \frac{1}{2} \left( \frac{dP}{dE} \right) E^2 + \Phi(E), \quad (\text{A1})$$

where  $\Phi(E)$  represents the scatter associated with point  $E$ . We assume  $\langle \Phi(E) \rangle \approx 0$ . Applying standard linear regression (see Press et al. 2002), we have

$$\begin{aligned} T'_0 &= \frac{S_{E^2} S_t - S_E S_{Et}}{SS_{E^2} - S_E^2}, \\ P' &= \frac{SS_{Et} - S_E S_t}{SS_{E^2} - S_E^2}, \end{aligned} \quad (\text{A2})$$

where

$$\begin{aligned} S_t &= \sum_{E \in \text{transits}} (t(E) / \sigma_{t(E)}^2) \\ &\approx \frac{1}{2} \left( \frac{dP}{dE} \right) S_{E^2} + P S_E + T_0 S, \\ S_{Et} &= \sum_{E \in \text{transits}} (t(E) E / \sigma_{t(E)}^2) \\ &\approx \frac{1}{2} \left( \frac{dP}{dE} \right) S_{E^3} + P S_E + T_0 S_E. \end{aligned} \quad (\text{A3})$$

We can then incorporate these expressions into Equation (A2) and separate out the terms involving  $dP/dE$  to arrive at Equation (33).

## ORCID iDs

Brian Jackson  <https://orcid.org/0000-0002-9495-9700>  
 Elisabeth R. Adams  <https://orcid.org/0000-0002-9131-5969>  
 Jeffrey P. Morgenthaler  <https://orcid.org/0000-0003-3716-3455>

## References

Aguilera-Gómez, C., Chanamé, J., Pinsonneault, M. H., & Carlberg, J. K. 2016, *ApJ*, 829, 127  
 Astropy Collaboration, Robitaille, T. P., Tollerud, E. J., et al. 2013, *A&A*, 558, A33

Astropy Collaboration, Price-Whelan, A. M., & Sipőcz, B. M. 2018, *AJ*, 156, 123  
 Bailey, A., & Goodman, J. 2019, *MNRAS*, 482, 1872  
 Barker, A. J. 2022, *ApJL*, 927, L36  
 Barros, S. C. C., Akınsanmi, B., Boué, G., et al. 2022, *A&A*, 657, A52  
 Baştürk, Ö., Southworth, J., Yalçınkaya, S., et al. 2023, *MNRAS*, 521, 1200  
 Behrard, A., Sevilla, J., & Fuller, J. 2023, *MNRAS*, 518, 5465  
 Bonomo, A. S., Desidera, S., Benatti, S., et al. 2017, *A&A*, 602, A107  
 Carter, J. A., Yee, J. C., Eastman, J., Gaudi, B. S., & Winn, J. N. 2008, *ApJ*, 689, 499  
 De, K., MacLeod, M., Karmelkar, V., et al. 2023, *Natur*, 617, 55  
 Deeg, H. J., Ocaña, B., Kozhevnikov, V. P., et al. 2008, *A&A*, 480, 563  
 Gu, P. G., Lin, D. N. C., & Bodenheimer, P. H. 2003, *ApJ*, 588, 509  
 Hagey, S. R., Edwards, B., & Boley, A. C. 2022, *AJ*, 164, 220  
 Hamer, J. H., & Schlaufman, K. C. 2019, *AJ*, 158, 190  
 Harre, J. V., Smith, A. M. S., Barros, S. C. C., et al. 2023, *A&A*, 669, A124  
 Harris, C. R., Millman, K. J., van der Walt, S. J., et al. 2020, *Natur*, 585, 357  
 Hunter, J. D. 2007, *CSE*, 9, 90  
 Ivshina, E. S., & Winn, J. N. 2022, *ApJS*, 259, 62  
 Jackson, B., Greenberg, R., & Barnes, R. 2008, *ApJ*, 678, 1396  
 Jackson, B., Jensen, E., Peacock, S., Arras, P., & Penev, K. 2016, *CeMDA*, 126, 227  
 Jia, S., & Spruit, H. C. 2017, *MNRAS*, 465, 149  
 MacLeod, M., Cantiello, M., & Soares-Furtado, M. 2018, *ApJL*, 853, L1  
 Mannaday, V. K., Thakur, P., Southworth, J., et al. 2022, *AJ*, 164, 198  
 Mayor, M., & Queloz, D. 1995, *Natur*, 378, 355  
 Metzger, B. D., Giannios, D., & Spiegel, D. S. 2012, *MNRAS*, 425, 2778  
 Ogilvie, G. I. 2014, *ARA&A*, 52, 171  
 Patra, K. C., Winn, J. N., Holman, M. J., et al. 2017, *AJ*, 154, 4  
 Patra, K. C., Winn, J. N., Holman, M. J., et al. 2020, *AJ*, 159, 150  
 Press, W. H., Teukolsky, S. A., Vetterling, W. T., & Flannery, B. P. 2002, *Numerical recipes in C++ : the Art of Scientific Computing* (Cambridge: Cambridge Univ. Press)  
 Qureshi, A., Naoz, S., & Shkolnik, E. L. 2018, *ApJ*, 864, 65  
 Rappaport, S., Sanchis-Ojeda, R., Rogers, L. A., Levine, A., & Winn, J. N. 2013, *ApJL*, 773, L15  
 Rasio, F. A., Tout, C. A., Lubow, S. H., & Livio, M. 1996, *ApJ*, 470, 1187  
 Rosário, N. M., Barros, S. C. C., Demangeon, O. D. S., & Santos, N. C. 2022, *A&A*, 668, A114  
 Schwarz, G. 1978, *AnSta*, 6, 461  
 Valsecchi, F., Rappaport, S., Rasio, F. A., Marchant, P., & Rogers, L. A. 2015, *ApJ*, 813, 101  
 Virtanen, P., Gommers, R., Oliphant, T. E., et al. 2020, *NatMe*, 17, 261  
 Vissapragada, S., Chontos, A., Greklek-McKeon, M., et al. 2022, *ApJL*, 941, L31  
 Weinberg, N. N., Sun, M., Arras, P., & Essick, R. 2017, *ApJL*, 849, L11  
 Winn, J. N. 2010, in *Exoplanets*, ed. S. Seager (Tucson, AZ: Univ. of Arizona Press), 55  
 Wong, I., Shporer, A., Vissapragada, S., et al. 2022, *AJ*, 163, 175  
 Yang, F., & Wei, X. 2022, *PASP*, 134, 024401  
 Yee, S. W., Winn, J. N., Knutson, H. A., et al. 2020, *ApJL*, 888, L5